ELSEVIER

Journal of Power Sources 112 (2002) 570–576

JOURNAL OF POWER SOURCES

www.elsevier.com/locate/jpowsour

# A combined passive water vapor exchanger and exhaust gas diffusion barrier for fuel cell applications

R.E. Williford*, B.K. Hatchell, P. Singh

*Pacific Northwest National Laboratory, P.O. Box 999, Mail Stop K2-44, Richland, WA 99352, USA*

Received 9 August 2002; accepted 19 August 2002

**Abstract**

Fuel cells operating on hydrocarbon fuels require water vapor injection into the fuel stream for fuel reforming and the prevention of carbon fouling. Compared to active water recovery systems, a passive approach would eliminate the need for a separate water source, pumps, and actuators, and thus reduce parasitic thermal losses. The passive approach developed in this paper employs a capillary pump that recovers the water vapor from the exhaust, while providing a diffusion barrier that prevents exhaust gases from entering the fuel stream. Benchtop proof tests have proven the feasibility of the passive fuel humidifier concept, and have provided a calibration factor for a computational design tool that can be used for industrial applications.



*Keywords:* Fuel cells; Fuel reforming; Water vapor exchanger; Efficiency; Models; Experiments

## 1. Introduction

Fuel cell systems that operate on hydrocarbon fuels such as natural gas require humidification of the fuel stream either for reforming or for prevention of hydrocarbon cracking that causes carbon fouling. Existing fuel cell systems utilize external water sources for humidification of the fuel stream, or capture water from the exhaust gas through active recirculation. Active recirculation as depicted in Fig. 1 requires high temperature valves, pumps, and construction materials that add to the overall system cost, as well as increasing the parasitic power loss. A high temperature recirculation system also adds to the volume and weight of mobile fuel cell systems.

The objective of this investigation was to develop a passive water vapor exchanger (labeled 'capillary humidifier' in Fig. 2) that would transfer water vapor from the solid oxide fuel cell (SOFC) exhaust stream to the fuel supply stream, while maintaining a liquid diffusion barrier between the two sides. The diffusion barrier prevents exhaust gases from entering and fouling the fuel stream, and is unique for this type of equipment.

A combined computational and experimental method was employed to develop this device. A computer code was written to simulate the vapor exchange process. Based on the calculations, a prototype device was built and tested under conditions easily attained in the laboratory. Comparison of results from the two methods allows calibration of the computational approach, which will subsequently be used to predict performance under other operating conditions, and to size the exchanger for industrial applications.

## 2. Description of computer simulation code

The computational approach employed standard and thus well documented engineering correlations [1] for mass transfer during condensation and evaporation of water vapor. The structure of the simulation code is shown by the flow diagram in Fig. 3, where an iterative solution method is outlined. The iterations proceed by assuming a temperature ($T_{ci}$) for the condensate/gas interface temperature on the condensor (SOFC exhaust) side. The mass flow rate of the condensed vapor ($m_c$) is computed from the mass flux coefficient ($K_c$) given by [1]

$$K_c = \frac{j_D G_m}{Sc^{2/3} P_{lm}}, \quad (1)$$

where $j_D$ is the correlation from curve 5 (for flat plates) shown in Fig. 30.1 of [1], $G_m$ the mass flow rate of the exhaust gas stream, $Sc$ the Schmidt number, and $P_{lm}$ is the

* Corresponding author. Tel.: +1-509-375-2956; fax: +1-509-375-2186.
*E-mail address:* rick.williford@pnl.gov (R.E. Williford).

0378-7753/02/$ – see front matter 
PII: S0378-7753(02)00454-8

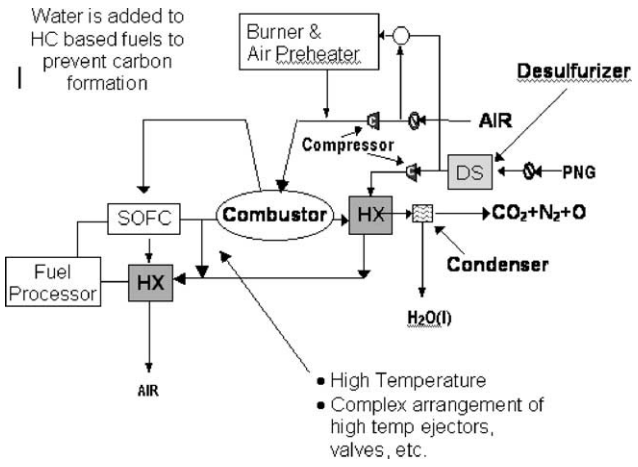


Fig. 1. Solid oxide fuel cell power generation system. This system includes a high temperature recirculation system to recycle CO and water from the exhaust to the fuel.

log mean pressure difference of the carrier gas (air in the experiments described later):

$$P_{\mathrm{lm}} = \left[\frac{P_{\mathrm{bulk}} - P_{\mathrm{interface}}}{\ln(P_{\mathrm{bulk}}/P_{\mathrm{interface}})}\right]_{\mathrm{air}}. \quad (2)$$

The interface pressure is defined by the temperature-dependent vapor pressure of water, for which a correlation was fitted to standard data [2]. The mass flow rate of condensate was computed from the pressure difference of the water vapor between the interface and the bulk gas stream:

$$m_{\mathrm{c}} = K_{\mathrm{c}}[P_{\mathrm{bulk}} - P_{\mathrm{interface}}]_{\mathrm{vapor}}. \quad (3)$$

The Chilton–Colburn analogy relates mass transfer to heat transfer, and was used to compute the heat transfer ($Q_{\mathrm{c}}$) across the capillary medium due to the condensation phase change. The temperature drop across the capillary medium ($\Delta T$) was then computed by assuming that heat transfer occurred through the parallel path presented by the water in the capillary pores (assumed to be spaced four pore radii apart on centers) and the stainless steel of the capillary medium. The capillary rise was computed using the Young–Laplace equation [3], and was found to be about 16 cm for this material under these conditions. This is more than adequate to 'pump' the condensed water from the condenser (exhaust) to the evaporator (fuel) side of the exchanger.

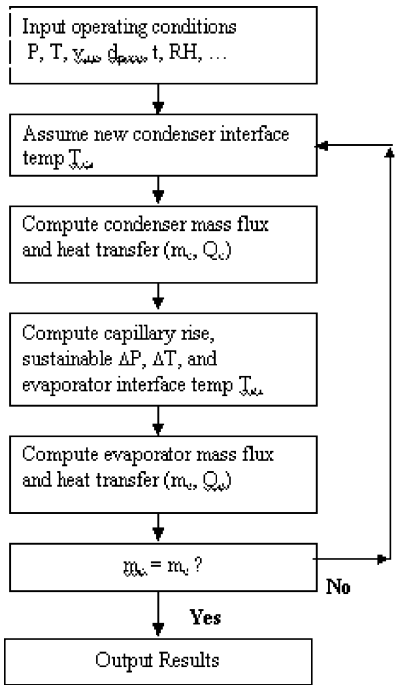


Fig. 3. Flow diagram of the computer code developed to simulate performance of the vapor exchanger.

The gas pressure ($\Delta P$) sustainable across the capillary medium was calculated using the same equation, and was found to be about 7 psi. This relatively high value is important for the operation of the vapor exchanger in industrial settings, where startup or load following conditions may cause pressure imbalances during transients. The capillary medium must be fully wetted at all times to prevent

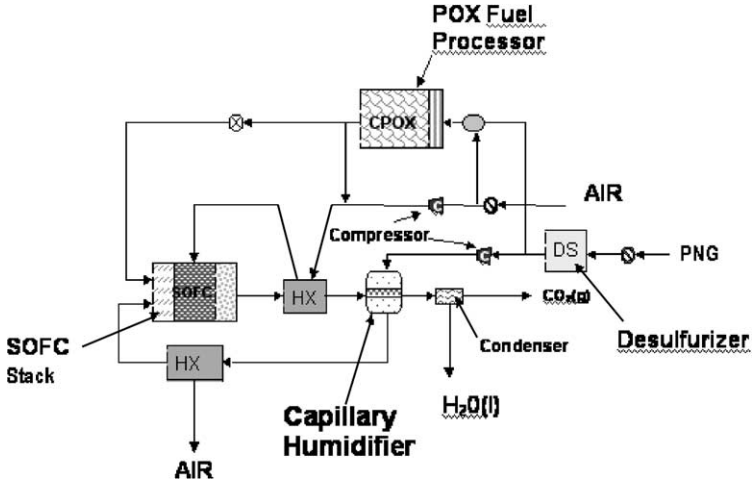


Fig. 2. Architecture of direct PNG SOFC power generation system.

the passage of exhaust gases into the fuel stream. A pressure difference above 7 psi would force the water from the capillaries, thus defeating the diffusion barrier. The high sustainable pressure difference allows the exchanger a certain degree of 'robustness' in practice.

Using the above temperature drop across the capillary medium (generally less than 1 °C), the water/gas interface temperature ($T_{ei}$) on the evaporator side is then computed, and subsequently used to calculate the evaporator mass flux ($m_e$) in a manner analogous to the condenser calculation shown earlier:

$$m_e = K_e(P_{interface} - P_{bulk})_{vapor}. \quad (4)$$

Again the associated heat transfer ($Q_e$) was computed using the Chilton–Colburn analogy. The two mass fluxes are then compared. If agreement is satisfactory, the code outputs the results. If there is disagreement, the iteration resumes with an improved estimate of the condenser interface temperature $T_c$.

The code simulates a counterflow exchanger, and performs the above calculations beginning at the location of the condenser (exhaust) input and evaporator (fuel) output. The iterative solution is found for a small segment of the exchanger, and the resulting gas compositions are used as input for the next segment. However, due to the small size of the sample tested, only one segment was necessary for these calculations. Axial heat flow considerations (along the flow streamlines) were limited to that transferred by the gases, and the solid capillary material was assumed to transfer heat only across its thickness.

It was assumed that the condensation and evaporation processes occurred from contiguous water films on the surface of the capillary medium. This assumption is supported by additional calculations which assumed that the evaporation occurred from the area of the capillary pores alone, rather than from a contiguous water film, and underestimated the experimental mass flux by factors of about 2. The water film assumption is also consistent with the large capillary rise reported earlier, which would ensure that excess water was always available on the evaporator side.

The agreement between the heat transfer from the condenser and evaporator sides of the exchanger using the water film assumption and the Chilton–Colburn analogy was within 4%, indicating that the above approach was successful. Finally, it should be noted that a second method for calculating condensation mass transfer was also employed for comparative purposes. The Colburn–Hougen method [4] noticeably underpredicted the condensate mass transfer, and was subsequently discarded.

## 3. Proof of principle experiments

Bench scale experiments were performed to test the passive humidifier concept and to obtain data for calibrating a computational model of the water exchanger. The test objectives, set-up, and results are discussed in this section.

The primary test objective was to measure the sustainable rate of water transfer between a dry air stream and a humid air stream separated by a porous capillary membrane. The test parameters, such as channel length, air velocity, and temperature, were chosen to permit a small benchtop test, and to provide meaningful data to calibrate the computational model. The processes of condensation and evaporation can occur at different rates and result in unsatisfactory circumstances. Excessive evaporation can lead to partial drying of the liquid barrier, and mixing between the gas streams. Excessive condensation can cause drop-wise condensation and moisture buildup in the exhaust line. Therefore, a process in which condensation is balanced with evaporation is highly desirable.

A secondary objective was to determine the maximum differential pressure that can be maintained between the two air streams by the porous capillary membrane. The fuel gas stream will be at a higher pressure than the exhaust, so the membrane must be able to sustain a pressure differential without compromising the diffusion barrier provided by the wetted membrane.

## 4. Experimental apparatus

A diagram of the test set-up is shown in Fig. 4. Small capacity air pumps with flow control valves (maximum flow rate 100 l/h) provided independent flow for both air streams. Tapered tube flow meters (Dwyer model VFB-50) were used to measure the flow rate of dry air. The condensing-side air stream was connected to a bubbler to raise the humidity to 100% to simulate the SOFC exhaust stream. Humidity sensors from the Controls Company were installed upstream and downstream of the condenser and evaporator sides to measure changes in temperature and humidity. The humid air and dry air streams were connected to the condenser and evaporator sides of the capillary humidifier, respectively, in a cross-flow arrangement, with the condensing side on the bottom.

The capillary humidifier consisted of a porous sintered stainless steel panel sandwiched between two Lexan® blocks (see Fig. 5). The panel was 2 μm grade, 0.062 in. (1.57 mm) thick and was procured from the Mott Corporation. Air passages were cut into both Lexan® blocks to create a channel 7 cm long with a 1 cm × 1 cm square cross-section. The capillary humidifier was partially submerged in hot water to increase the temperature and saturation pressure of the air and to generate a temperature gradient across the membrane panel (Fig. 6), thus simulating the fuel-exhaust temperature gradient in a SOFC.

Prior to testing, the evaporator outlet was plugged and a small amount of water was introduced to the evaporator side of the capillary humidifier. The evaporator side was then pressurized to approximately 1 psi to infuse water into the membrane. The Mott Corporation recommended this pre-wetting procedure for wicking applications. For

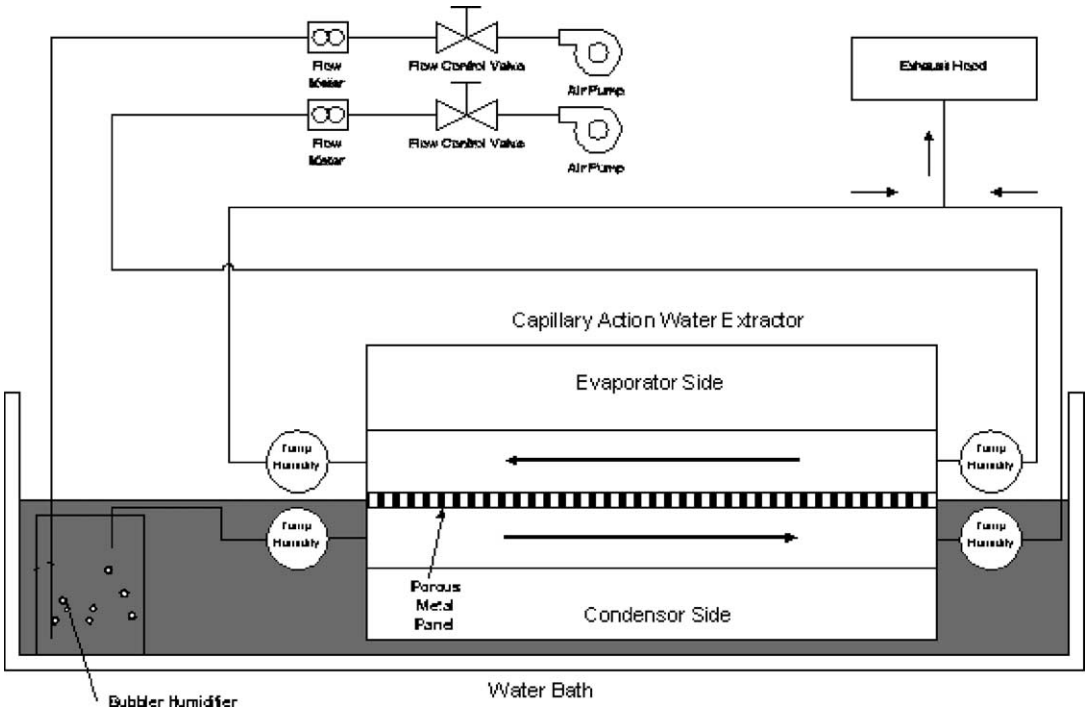


Fig. 4. Micro-capillary humidifier test schematic.

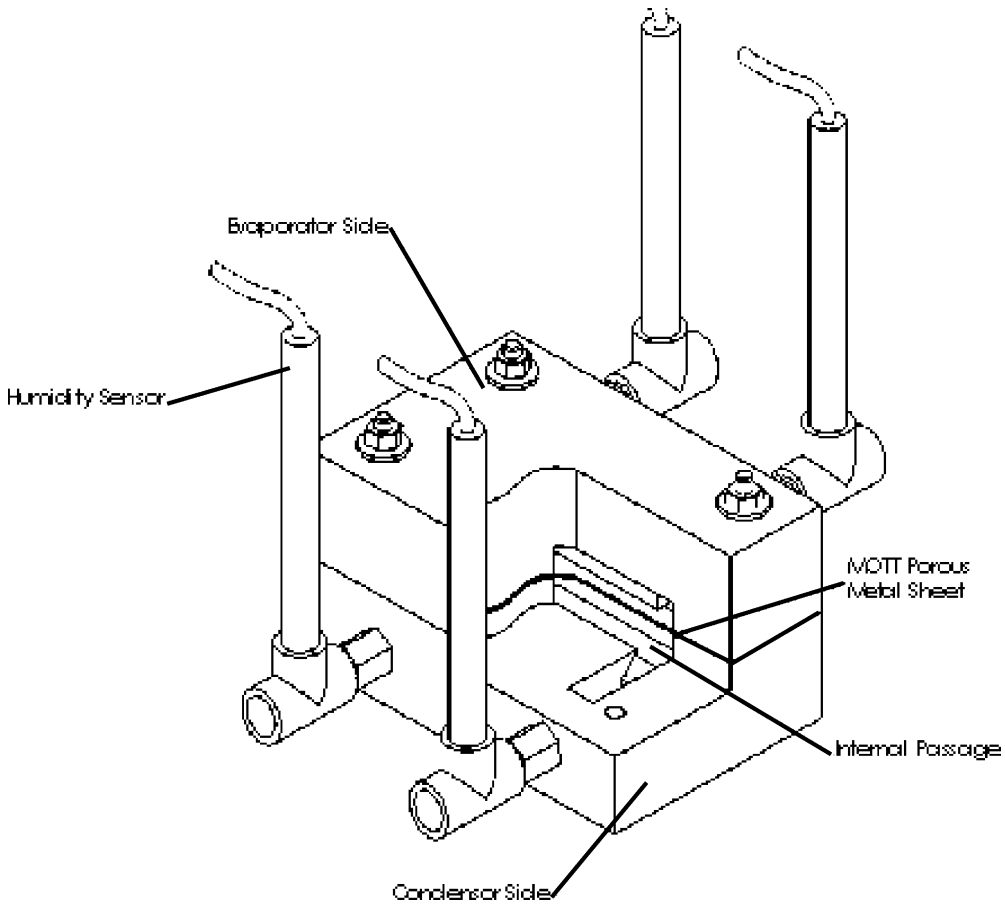


Fig. 5. Section view of the test humidifier. The humidifier was fabricated with a porous metal sheet sandwiched between two Lexan® blocks with internal passages.

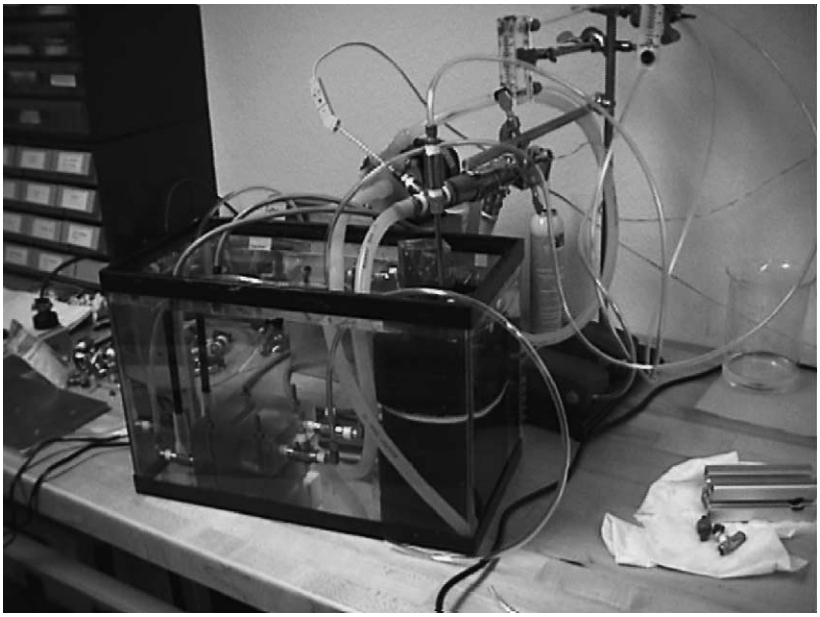

Fig. 6. Prototype humidifier partially submerged in a water bath to create a temperature gradient across the capillary membrane.

each set point, the evaporator was operated for at least 20 min to allow the process to reach steady-state conditions.

## 5. Comparison of test results with model predictions

Results from three proof test experiments are shown in Tables 1–3 and performance is summarized in Figs. 7 and 8. For the first and second experiments (cases 1 and 2), the flow rate of dry air was held constant at 1.5 SCFH and 3.0 SCFH, respectively, on both the condenser and evaporator sides of the humidifier. For the third case, the flow rate of dry air was 3 SCFH on the evaporator side and 1.5 SCFH on the condenser side. The water bath temperature was maintained

Table 2
Results from the second experiment

| Case 2 | Condenser (exhaust side) | Evaporator (fuel side) |
|---|---|---|
| Air velocity (cm/s) | 23.6 | 23.6 |
| Air pressure (atm) | 1.09 | 1.05 |
| Air temperature (°C) | 44.7/44.7 | 33.1/33.1 |
| Air/liquid interface temperature (°C)—predicted | 39.0 | 38.5 |
| Mole fraction of water—inlet | 0.0961/0.0961 | 0.0107/0.0207 |
| Mole fraction of water—outlet | 0.0707/0.0775 | 0.0405/0.0405 |
| Mass flow rate (g/min) | 0.0314/0.0215 | 0.0326/0.0215 |
| Prediction error (%) | −31 | −34 |
| Exchange rate (SLPM) | 0.0292 | 0.0292 |
| Sustainable pressure (psi) | 7.2 | 7.2 |

Table entries are given as experimental/predicted where appropriate.

Table 1
Results from the first experiment

| Case 1 | Condenser (exhaust side) | Evaporator (fuel side) |
|---|---|---|
| Air velocity (cm/s) | 11.8 | 11.8 |
| Air pressure (atm) | 1.10 | 1.08 |
| Air temperature (°C) | 46.4/46.0 | 42.6/42.0 |
| Air/liquid interface temperature (°C)—predicted | 42.7 | 42.3 |
| Mole fraction of water—inlet | 0.1048/0.1048 | 0.0117/0.0251 |
| Mole fraction of water—outlet | 0.0692/0.0739 | 0.0578/0.0578 |
| Mass flow rate (g/min) | 0.0222/0.0178 | 0.0257/0.0178 |
| Prediction error (%) | −19 | −31 |
| Exchange rate (SLPM) | 0.0243 | 0.0243 |
| Sustainable pressure (psi) | 7.08 | 7.08 |

Table entries are given as experimental/predicted where appropriate.

Table 3
Results from the third experiment

| Case 3 | Condenser (exhaust side) | Evaporator (fuel side) |
|---|---|---|
| Air velocity (cm/s) | 11.8 | 23.6 |
| Air pressure (atm) | 1.09 | 1.05 |
| Air temperature (°C) | 44.4/44.4 | 33.3/33.3 |
| Air/liquid interface temperature (°C)—predicted | 37.5 | 36.9 |
| Mole fraction of water—inlet | 0.0937/0.0937 | 0.0104/0.0109 |
| Mole fraction of water—outlet | 0.0634/0.0532 | 0.0325/0.0325 |
| Mass flow rate (g/min) | 0.0186/0.0233 | 0.0239/0.0233 |
| Prediction error (%) | +25 | −2 |
| Exchange rate (SLPM) | 0.0316 | 0.0316 |
| Sustainable pressure (psi) | 7.2 | 7.2 |

Table entries are given as experimental/predicted where appropriate.

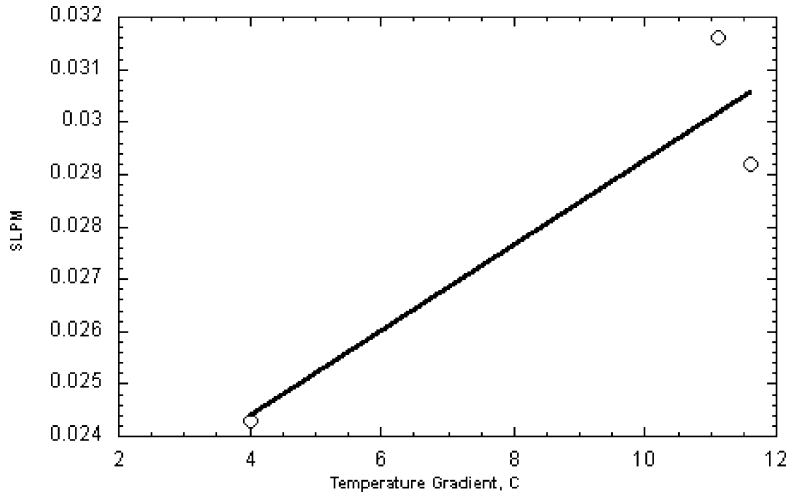


Fig. 7. Predicted exchanger performance plotted as standard liters per minute (SLPM) of water vapor exchanged vs. the temperature difference between condenser (exhaust) and evaporator (fuel) flow stream bulk temperatures. Solid line: prediction; open circles: experimental data.

at 50 °C. The humidity level decreased on the condenser side and increased on the evaporator side, as expected. The rate of water transport was between 3 and 22% higher on the evaporator side, indicating that evaporation was more efficient than condensation. Sustainable pressure differentials were in agreement with calculations.

As expected, exchanger performance increases with the temperature difference from the condenser to evaporator sides (Fig. 7). This is consistent with the Chilton–Colburn analogy, which relates the heat transfer to the mass transfer. Since heat transfer increases with temperature difference, so would the mass transfer.

Fig. 8 provides the most useful information for calibrating the design code. There it can be seen that the evaporator is more efficient than the condenser, since the former has a higher mass transfer rate than the latter. The expectation is that the evaporator side will require a smaller temperature gradient (from the water/vapor interface to the bulk gas stream) to produce the same mass flux as the condenser. This is advantageous because the SOFC inlet fuel temperature is much easier to control than the exhaust.

The simulation code underpredicted the experimental performance by about 28% on the average. This would imply that a calibration factor of about 1.28 should be applied to the mass transfer calculations when sizing the exchanger for industrial applications. This relatively small correction factor is an encouraging result, considering the experimental uncertainties and the approximate nature of the 'universal' mass transfer correlation employed. In addition, the design code has been constructed for incremental calculations along the flow path, so more accurate calculations can be performed as needed for sizing the device. Alternative exchanger designs, such as tube

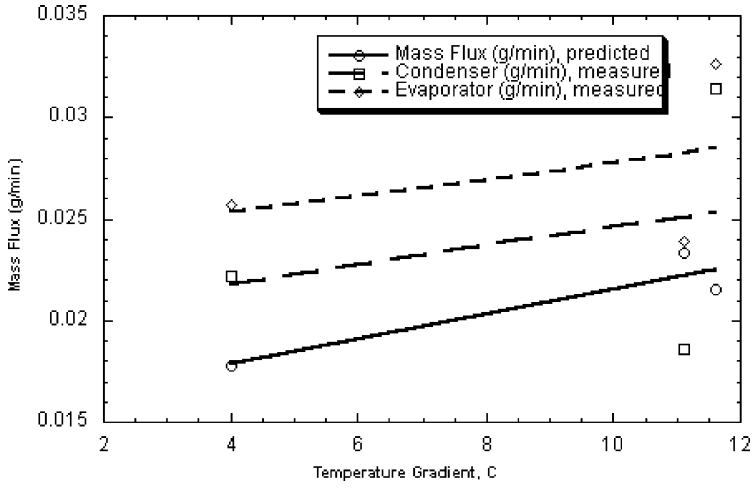


Fig. 8. Predicted (lines) and measured (symbols) exchanger performance plotted as mass flux (g/min) exchanged vs. the temperature difference between condenser (exhaust) and evaporator (fuel) flow stream bulk temperatures.

in shell configurations, can be investigated by simply employing the appropriate mass transfer correlation from Table 30.1 of [1]. An invention disclosure has been filed for this device.

## 6. Conclusions

A passive water recovery approach has been developed for advanced SOFC power generation systems using hydrocarbon fuels. The approach has the potential to eliminate the need for a separate water source, pumps, and actuators, and thus to reduce parasitic thermal losses. The passive humidifier developed herein is based on a capillary pump that recovers water vapor from the fuel stream, while preventing exhaust gases from entering the fuel. Test results have proven the feasibility of the passive humidifier concept, and have provided a calibration factor for a computational design tool that can be used for industrial applications.

## Acknowledgements

This work was performed as part of the Laboratory Directed Research and Development program at Pacific Northwest National Laboratory, which is operated for the US Department of Energy by Battelle Memorial Institute under contract DE-AC06-76RLO-1830.

## References

[1] J.R. Welty, C.E. Wicks, R.E. Wilson, Fundamentals of Heat, Mass and Momentum Transfer, Wiley, New York, 1969, Chapter 30.
[2] D.R. Lide, CRC Handbook of Physics and Chemistry, 76th ed., CRC Press, New York, 1995.
[3] I.N. Levine, Physical Chemistry, McGraw-Hill, New York, 1988, p. 363.
[4] A.P. Colburn, O.A. Hougen, Ind. Eng. Chem. 26 (11) (1934) 1178–1182.